The Astrophysical Journal, 649:1028–1042, 2006 October 1

SPITZER 24 μm SURVEY OF DEBRIS DISKS IN THE PLEIADES

Nadya Gorlova,[1] George H. Rieke,[1] James Muzerolle,[1] John R. Stauffer,[2] Nick Siegler,[1]
Erick T. Young,[1] and John H. Stansberry[1]
Received 2006 February 27; accepted 2006 June 1

ABSTRACT

We performed a 24 μm $2^\circ \times 1^\circ$ survey of the Pleiades cluster, using the MIPS instrument on *Spitzer*. Fifty-four members ranging in spectral type from B8 to K6 show 24 μm fluxes consistent with bare photospheres. All Be stars show excesses attributed to free-free emission in their gaseous envelopes. Five early-type stars and four solar-type stars show excesses indicative of debris disks. We find a debris disk fraction of 25% for B–A members and 10% for F–K3 ones. These fractions appear intermediate between those for younger clusters and for the older field stars. They indicate a decay with age of the frequency of the dust production events inside the planetary zone, with similar timescales for solar-mass stars as have been found previously for A stars.

Subject headings: circumstellar matter — infrared: stars — open clusters and associations: individual (Pleiades) — planetary systems: formation

1. INTRODUCTION

After a few hundred million years, a planetary system is expected to have assumed its final configuration and has either set the stage for life, or will probably remain barren forever. It is difficult to probe this era. Most of its traces have been obliterated in the solar system. Only a minority of the nearby stars are so young. Even for them, planets—and particularly those in the terrestrial planet/asteroidal region—are faint and are lost in the glare of their central stars. However, when bodies in this zone collide, they initiate cascades of further collisions among the debris and between it and other members of the system, eventually grinding a significant amount of material into dust grains distributed in a so-called debris disk. Because the grains have larger surface area per unit mass compared to larger bodies, they (re)radiate more energy and therefore are more easily detected in the IR compared to their parent bodies. By studying this signal, we can probe the evolution of other planetary systems through this early, critical stage.

Debris disks are found around stars generally older than $\sim$10 Myr, with no signs of gas accretion (as judged from the absence of emission lines or UV excess) (Lagrange et al. 2000; Hillenbrand 2005). In the absence of gas drag, a 10 μm sized dust grain from the primordial, proto–planetary nebula cannot survive longer than $\sim$1 Myr within 10 AU of a star due to a number of clearing processes, such as sublimation, radiation pressure, Poynting-Robertson, and stellar wind drag (Backman & Paresce 1993; Chen et al. 2005a). Therefore, any main-sequence star older than 10 Myr with an IR excess is a candidate to have circumstellar material supplied through debris disk processes.

In our solar system there are two main sources of dust: colliding asteroids and evaporating comets. The dust (grains <1 mm in size) is concentrated in two belts—the asteroid belt at 2–3.5 AU, $L_{\rm dust} = 10^{-7}\ L_\odot$, $T_{\rm dust} = 150$–200 K, $M_{\rm dust} = 10^{-8}\ M_\oplus$ (Low et al. 1984; Dermott et al. 2002; Hahn et al. 2002); and the Kuiper belt at 30–50 AU, $L_{\rm dust} = 10^{-7}\ L_\odot$, $T_{\rm dust} = 40$–100 K, $M_{\rm dust} = 10^{-5}\ M_\oplus$ (Backman et al. 1995; Morbidelli et al. 2003). Asteroid collisions that produce warm dust are driven by perturbations by planets, a process that has cleared most of the interplanetary material from the inner 30 AU of the system. In contrast, there is substantial mass in the Kuiper Belt, concentrated in reasonably stable structures controlled by giant planets (Liou & Zook 1999; Moro-Martín & Malhotra 2002). Similarly, rings, blobs, warps, and other nonuniformities are frequently observed in the spatially resolved images of nearby extrasolar debris disks and inferred from the spectral energy distributions in the distant unresolved disks, implying the presence of *planetary-mass bodies* in these systems.

The first debris disks were discovered by the *Infrared Astronomical Satellite* (*IRAS*) in the 1980s. Only a handful of nearby ones have been resolved in optical and near-IR (NIR) scattered light or detected in submillimeter thermal emission; the *Infrared Space Observatory* (*ISO*) has extended the *IRAS* results, but only to a modest extent (e.g., Laureijs et al. 2002). The limited sensitivity of *IRAS* and *ISO* and the even more severe limitations of other methods have prevented a complete census, particularly to photospheric emission levels. In addition, some alleged disks have been confused with background objects or cirrus in the large beam of *IRAS*. The attempt to assess the percentage of stars with debris disk emission therefore appeared premature from pre-*Spitzer* data (Zuckerman 2001).

With superior sensitivity and a smaller beam size, *Spitzer* is providing many new insights to debris disk behavior. For example, Rieke et al. (2005) demonstrated both the overall decline of debris disks with age (first noted in Holland et al. [1998] and Spangler et al. [2001]) and the large scatter of disk properties at any given age (as previously noted in Decin et al. [2003]). By probing excesses to within 25% of the photospheric emission, Rieke et al. (2005) found a surprising number of nonexcess stars even at ages as young as 10–20 Myr, implying very rapid clearing of the inner 10–60 AU region in these systems.

The study of Rieke et al. (2005) was purposely confined to A stars, with masses $\sim$2.5 $M_\odot$. It poses the question of whether the same patterns of disk evolution hold for less massive stars, especially in the *solar*-mass range—spectral types FGK. The study of excesses in young solar analogs could corroborate lunar geological evidence of the bombardment history in the solar system. Two major surveys of solar-type stars in the field are under way with *Spitzer*—the solar star survey by the Multiband and Imaging Photometer for *Spitzer* Guaranteed Time Observers (MIPS

[1] Steward Observatory, University of Arizona, 933 North Cherry Avenue, Room N204, Tucson, AZ 85721-0065; ngorlova@as.arizona.edu.
[2] *Spitzer* Science Center, California Institute of Technology, MS 314-6, Pasadena, CA 91125.

GTO) team, searching for disks around ~150 field stars within 25 pc (Bryden et al. 2006), and the Legacy Survey by the Formations and Evolution of Planetary Systems (FEPS) group, searching for disks around ~330 stars, both field and members of nearby open clusters and associations (Meyer et al. 2004). Interpretation of these surveys is still in progress; nevertheless, preliminary results indicate that among solar analogs typically older than 1 Gyr ~10%–15% have excess emission at 70 μm, indicative of Kuiper Belt analogs ~10–100 times more massive than in the solar system (Kim et al. 2005; Bryden et al. 2006). On the other hand, 24 μm excesses that would be indicative of massive zodiacal belts are much more rare around these stars: ~1% (Beichman et al. 2005, 2006).

To explore younger systems with good number statistics and small uncertainties in age determination, an open cluster survey has been initiated by the MIPS and Infrared Array Camera (IRAC) GTO groups. The first clusters studied in this program were the 25–35 Myr old NGC 2547 (Young et al. 2004) and the 60–100 Myr old M47 (NGC 2422) (Gorlova et al. 2004). At 24 μm photospheres were detected in NGC 2547 down to mid-F and in M47 to early G spectral types, beginning to probe disks in the solar-mass regime. A decrease with age in both the amount and the fraction of excess (from ~40% to 25%) is indicated for B–A stars between the two clusters (as included in Rieke et al. [2005]). For F-K stars a similar trend is only suggested: quantitative estimates are impossible because photospheres start dropping below the detection limit. Thus, it is not clear whether the high incidence of 24 μm excesses around A stars is a product of their high luminosities and efficiency in heating dust, or simply results because they are by definition relatively young ($<$1 Gyr).

To probe the evolution of debris disks around solar-mass stars, we have investigated the Pleiades. The Pleiades is one of the best-studied clusters with membership extending into the substellar regime (e.g., Moraux et al. 2003; Pinfield et al. 2003). At 24 μm *Spitzer* is potentially sensitive enough to detect photospheres in this cluster down to early M spectral type. To exploit these advantages, one must contend with an interstellar cloud of gas and dust, whose thermal emission beyond 10 μm dominates over starlight in the southwest part of the cluster. There is no consistent picture of the structure and kinematics of this nebulosity, except that it might be a part of the ~10 Myr Taurus-Auriga star-forming complex through or behind which the Pleiades happens to be passing at the present epoch (e.g., Breger 1987). Recent studies, however, agree that at least some of the material is located within the cluster and possibly interacts with the brightest members (Gibson & Nordsieck 2003; White 2003). Dust in the molecular cloud is sheared by the radiation pressure and assembles into filaments that wrap around stars, forming a characteristic pattern of reflection nebulosity known as the "Pleiades phenomenon" (Arny 1977; Herbig & Simon 2001). The unresolved thermal emission from the interstellar dust shell can mimic emission from a debris disk, as was, for example, demonstrated with coronagraphic imaging of the *IRAS*-selected Vega-like stars by Kalas et al. (2002). Special measures were undertaken in our survey to avoid confusion with interstellar dust (§§ 2–3).

Pre-*Spitzer* IR and submillimeter (Zuckerman & Becklin 1993) searches for Pleiades disks were largely unsuccessful. The few reported detections by *IRAS* (Castelaz et al. 1987) and the *Midcourse Space Experiment* (Kraemer et al. 2003) concerned the brightest B-type members, which we find to be either surrounded by heavy cirrus or emission-line stars with gaseous disks. Spangler et al. (2001) observed 14 low-mass members with *ISO*, and claim detection (and excesses) at 60 and/or 90 μm in the two G0 and K2 members HII 1132 and HII 3163. The fractional dust luminosity in these stars, if accurate, is unusually high, about 10^{-2}, comparable to the transitional disks found around $\lesssim$10 Myr old stars. Unfortunately, both stars are outside of our *Spitzer* fields. Recently Stauffer et al. (2005), within the framework of the FEPS project, investigated 19 solar-type members outside of the cluster core. They found excess emission at 24 μm at levels up to 40% above the photosphere in a few members. Compared to the FEPS study, ours is centered on the cluster core, covers a larger area, and considers all members independent of spectral type or binarity. It is a magnitude- and background-limited survey based on the membership derived from the optical studies. For the first time, it provides adequate number statistics to constrain the disk incidence around Pleiades members similar in mass to the Sun.

2. OBSERVATIONS AND DATA REDUCTION

The Pleiades were imaged with the MIPS instrument in the scan map mode with half-pixel subsampling (Rieke et al. 2004). One area of size $90' \times 60'$ was centered on the cluster core, as defined by the "seven sisters" (the brightest B-type members) and the associated reflection nebula. It was observed in two segments in 2004 February. Another field of size $75' \times 45'$, centered approximately $75'$ north of the cluster core, was observed in 2004 September. All the observations were done using medium scan mode with half-array cross-scan overlap, resulting in a total effective exposure time per point at 24 μm of 80 s. The 24 μm images were processed using the MIPS instrument team Data Analysis Tool, which calibrates the data and applies a distortion correction to each individual exposure (Gordon et al. 2005). We further applied a column-dependent median subtraction routine to remove a small residual dark latent pattern from individual images before combining into a final mosaic. Data at 70 and 160 μm were taken simultaneously; however, the images yielded no detections of interest to this study because of the sensitivity limits and strong background cirrus, and we will not discuss them further.

The thermal emission from the nebula is strongest in the west side of the cluster, where the interstellar medium (ISM) cloud is of highest density, as indicated by the enhanced extinction, polarization, and detection of CO gas (Breger 1987). This highly nonuniform nebulosity limits our ability to perform photometry on the faint sources in the central field to only those that are situated in the clean gaps between the bright filaments. The northern field contains fewer members, being farther from the cluster core, but it has the most uniform background. We performed photometry independently on each field, which allowed us to evaluate the uncertainty of our photometry based on the objects from the overlapping regions ~$5'$ wide. The full area of our survey is shown in Figure 1. The image was created by merging all three fields with the IRAF task `imcombine`, after applying appropriate offsets to account for the different levels of zodiacal light in each field. Stars marked in the figure outside the map boundaries are from Stauffer et al. (2005).

The complicated background required an investigation of the optimum way of doing photometry. We carried out two tests to find parameters that provide the most accurate results for aperture and point-spread function (PSF)–fitting photometry. Standard IRAF tasks `phot` and `allstar` from the `daophot` package were used. The first test compared the difference between the input and the recovered flux of artificial stars, inserted into different background environments (using task `addstar`). The second test looked at the tightness of the locus of the cluster members on the $J-H$ versus $K-[24]$ diagram. For the nonexcess stars, we assumed that the dispersion is dominated by the measurement errors in the 24 μm flux, since reddening is negligible at these

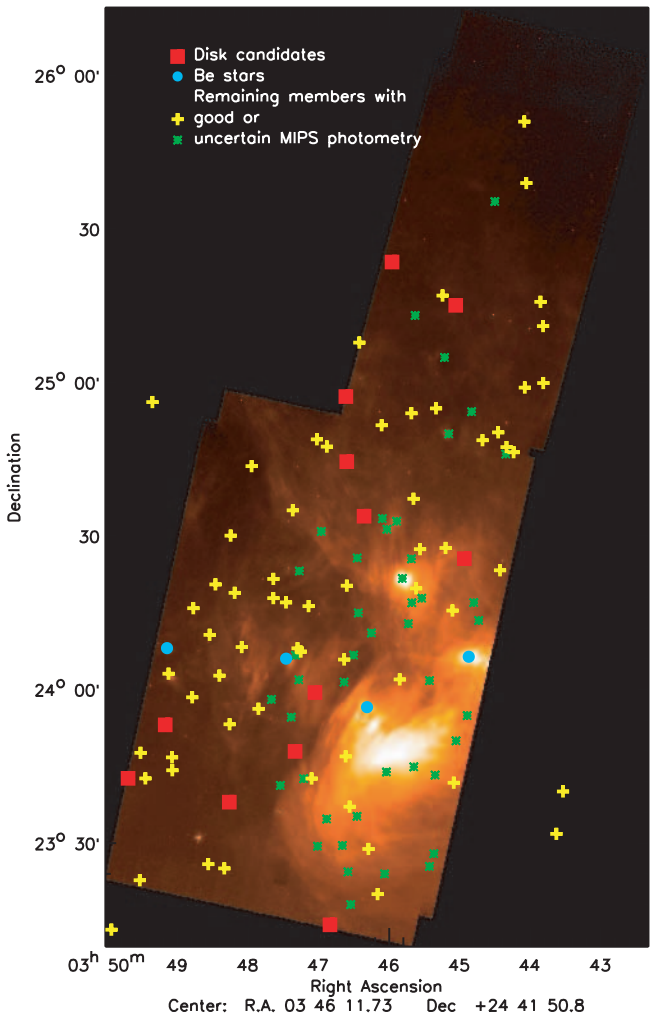

FIG. 1.—MIPS 24 μm mosaic made of three scan maps. *Plus signs*: Pleiades members with 24 μm images allowing accurate PSF-fitting photometry, from this work and Stauffer et al. (2005), also listed in Table 2. *Squares*: Debris disk candidates, marked by asterisks in Table 2. *Asterisks*: Pleiades members with 24 μm images contaminated by cirrus or a nearby source, listed in Table 1. *Circles*: Be stars, all of them formally showing excess, a mix of pointlike and extended sources.

wavelengths. We tried a range of aperture radii starting with the HWHM of the MIPS beam of 2.3 interpolated pixels (1 pixel = 1.″247) and a range of sky annuli centered at the first Airy ring at 7 pixels. We finally adopted PSF-fitting photometry with a small value for the fitting radius of 3 pixels and a close sky annulus with inner and outer radii of 5 and 10 pixels, respectively. The PSF template for all three fields was constructed from nine stars in the north field, carefully selected to be in the regions clear of nebulosity and to have a representative range of magnitudes. As a check, another PSF was created from seven "clean" stars eastward from the cluster center. Magnitudes of the PSF stars measured with both PSFs agree to within 0.01 mag.

To determine an aperture correction, we compared magnitudes within an aperture radius of 3.5 pixels for the nine PSF stars performed with our adopted *PSF-fitting* photometry to the *aperture* photometry with parameters that would normally be used on a uniform background-aperture radius equal to the FWHM of the beam (4.6 pixels), sky annulus beyond the first Airy ring (12 and 18 pixels for the inner and outer radii), and aperture correction of 0.68 mag from 4.6 pixels to infinity (as established by the MIPS team based on the STinyTim simulated PSF). The resulting aperture correction for our Pleiades-customized PSF-fitting photometry is 0.89 mag. Finally, to translate fluxes in number counts into 24 μm magnitudes, we use a conversion factor of 1.627×10^{-6} Jy(DN s^{-1})$^{-1}$ (where DN is the data number per pixel, for 1.″25 pixels). We took 7.3 Jy for the [24] magnitude zero point.

Two cluster members (HII 1284 and HII 1380), of $[24] \approx 7$ mag (or $\sim$10 mJy) appear on both east and west subfields, providing a consistency check of the photometric errors calculated by `allstar`. Their magnitudes differ between the two subfields by 0.08 and -0.01 mag, respectively (with the larger difference for HII 1284 most certainly due to a faint companion; see § 5.3). We also detect six members in common with Stauffer et al. (2005) (HII 173, HII 174, HII 250, HII 314, HII 514, and HII 2147). The average difference between our MIPS [24] magnitudes and those of Stauffer et al. is -0.02, rms = 0.10 mag. We have four early-type stars in common with Rieke et al. (2005) (HII 1431, HII 1823, HII 1876, and HII 2425); comparison with updated photometry (K. Y. L. Su 2006, private communication) indicates 0.07 mag difference between us and the latter work, with rms = 0.04 mag. We conclude that the random error of our 24 μm photometry is about 5% for objects brighter than $\sim$2 mJy in the clean regions of the sky, which is consistent with the scatter seen in the $K-[24]$ color of the nonexcess members (§ 4). The systematic error in our data calibration is of similar magnitude (few percent), consistent with comparisons of objects common to other independent studies.

3. SAMPLE

We measured the 24 μm fluxes of the Pleiades members as follows. Using the `daophot` task `find` and visual inspection, for each MIPS field we constructed an initial coordinate list for all discernible pointlike sources. Task `phot` provided initial aperture photometry, which served as input for the PSF-fitting photometry with `allstar`. Task `allstar` was executed with the recentering option turned on. Next, the `allstar` coordinates were correlated with the Two Micron All-Sky Survey (2MASS) point-source catalog, with a search radius of 2.″5. Using the 2MASS designations, we identified Pleiades members using an online catalog of the highly probable members maintained by J. Stauffer. Tables 1 and 2 summarize our measurements as well as some catalog properties for these sources. The information on binarity was supplemented with data from Liu et al. (1991) and Raboud & Mermilliod (1998). Table 2 also contains measurements from Stauffer et al. (2005) for 13 members outside of our field of view.

Meaningful PSF photometry cannot be performed if the sky level is highly variable within the fitting region, or if the object's shape deviates significantly from an Airy function with the adopted FWHM. Also, compact cirrus falling within the 6″ MIPS beam (corresponding to 800 AU at the Pleiades distance of 133 pc) can mimic radiation from an unresolved debris disk. To exclude ambiguity in the photometry, we examined the image of every detected member. We designate as problematic objects having either a nonuniform (filamentary or curved) background within $\sim$15 pixels of the target (1.5 times the region of sky fitting) or a bright companion contaminating the target aperture. For the sources that passed this test, we generated radial profiles and rejected any with FWHM $\gtrsim$ 5 pixels (6.″2). These problematic sources are listed in Table 1, and examples are shown in Figure 2; in Figures 1 (except for Be stars) and 3 they are designated by asterisks. Most of them cluster around the ridge of dense ISM clouds in the west part. For a number of them (marked by asterisks in Table 1) the formal procedure of PSF fitting indicates considerable excesses. Whether these excesses are real and due to debris disks

TABLE 1

PLEIADES MEMBERS WITH CONTAMINATED 24 μm PHOTOMETRY

Name	$(V-K)_0$[a] (mag)	[24] Flag[b]	Spectral Type	A_V (mag)	$v \sin i$ (km s^{-1})	Binary?	2MASS
HII 0468*	−0.25*	h*	B6 IIIe*	0.04*	220*	SB1?*	03445253+2406478*
HII 0785	−0.24	h	B7 III	0.16	40	OccB	03454960+2422037
HII 0541*	−0.24*	h*	B8 V*	0.09*	245*	SB?*	03450973+2450213*
HII 0980*	−0.22*	me*	B6 IVe*	0.21*	275*	B?*	03461958+2356541*
HII 0447	−0.20	h	B7 IV	0.19	260	OccB	03444821+2417222
HII 0817*	−0.16*	h*	B8 V*	0.16*	220*	...	03455447+2433162*
HII 0859*	−0.13*	h*	B9 V*	0.15*	250*	...	03460288+2431403*
HII 1234*	−0.10*	h*	B9.5 V*	0.26*	260*	VB	03465940+2431124*
HII 1375*	0.03*	me*	A0 V*	0.00*	160*	SB*	03472103+2406586*
HII 1397	0.12	cc	A2 V	0.00	<10	SB1, VB 6.26[c]	03472440+2354529
HII 1028*	0.18*	me*	A2 V*	0.05*	110*	SB?*	03462728+2415181*
HII 0652*	0.35*	h*	A3 V*	0.26*	235*	SB?*	03452613+2402065*
HII 0956*	0.76*	me*	A7 V*	0.10*	150*	SB?*, VB*	03461600+2411234*
HII 0745	1.05	b	F5 V	0.40	65	SB1?	03454138+2417189
HII 0476	1.19	b	F9	0.87	21	PHB, SB	03445383+2355165
HII 0761	1.35	b	G2	0.50	11	SB1	03454440+2413132
HII 1215	1.46	b	G0	0.11	6	...	03465373+2335009
HII 0320*	1.63*	cc*	G5*	0.61*	11*	SB1*	03442050+2446222*
HII 0659*	1.68*	b*	G4*	0.74*	12*	...	03452597+2325487*
HII 0746	1.72	b	G5	0.20	5	SB?	03454184+2425534
HII 0870	1.78	b	G4.5	1.77	10	VB 0.51[c]	03460275+2344146
HII 1275	1.78	b	G8	0.15	6	...	03470141+2329419
HII 1032	1.84	b	G8	0.11	36	...	03462841+2426021
HII 0430*	1.84*	b*	G8*	0.09*	7*	...	03444398+2413523*
HII 1136	2.23	b	G8	0.68	68	...	03464024+2329520
HII 1124	2.24	b	K1	0.25	6	...	03463938+2401468
HII 0522	2.24	b	K2	0.00	4	SB1	03450326+2350219
HII 0625	2.27	b	K0	1.15	94	...	03452118+2343389
HII 0738*	2.30*	b*	G9*	1.12*	50*	VB 0.50*[c]	03453940+2345154*
HII 1039	2.40	b	K1	0.84	<5	...	03462777+2335337
HII 1332	2.52	b	K4	0.00	5	...	03471352+2342515
HII 0636	2.55	b	...	...	4	...	03452219+2328182
HII 0883	2.80	b	...	...	4	...	03460689+2433461
HII 0882	2.98	b	K3	0.15	65	...	03460412+2324199
HII 1348	2.98	b	K5	0.00	5	SB2	03471806+2423267
HII 0451	3.09	b	K5	0.06	6	...	03445017+2454400
HII 0559	3.11	b	...	...	65	...	03451352+2505159
HII 1061*	3.20*	b*	K5*	0.62*	7*	VB 0.32*[c]	03463117+2407025*
HII 0686	3.23	b	K7	0.06	64	...	03453293+2418116
HII 1531	3.27	b	K7.5	0.00	50	...	03474143+2358190
HII 1081	3.44	b	K6	0.40	<10	...	03463287+2318191
HII 1355	3.45	b	K6n	0.34	12	VB 1.26[c]	03471814+2402114
HII 1103	3.73	b	K7	0.34	18	...	03463532+2324424
HCG 0196	3.82	b	...	...	...	...	03453903+2513278
HCG 0152	4.03	b	...	...	...	...	03443006+2535470
HCG 0277	4.84	b	...	...	...	...	03473345+2341330

NOTES.—Objects sorted according to $(V-K)_0$. Sources with nominal 24 μm excesses are marked by asterisks.

[a] Dereddened where spectral type available.

[b] me = marginally extended source; FWHM = 6.″5–7″; h = a halo-like extended smooth cirrus, with or without point source on top; b = within strongly nonuniform background; cc = close companion.

[c] In units of arcseconds.

or an artifact of cirrus contamination remains to be seen with better resolution. The analysis presented in the rest of the paper only deals with members that passed the above contamination test. These clean sources are shown in Table 2 and in Figure 4.

As a measure of the 24 μm excess we use a $K-[24]$ color (where K is a 2MASS K_S). Since there is no NIR excess, as expected for stars of age $\sim$100 Myr, the K-band flux represents the photospheric flux. The K band is the least affected by reddening of the three 2MASS bands. On average, the extinction toward the Pleiades is small, $\langle A_V \rangle \approx 0.1$ mag. However, it may exceed 1 mag in the southwest, the densest part of the interstellar cloud (Breger 1986, 1987; Stauffer & Hartmann 1987; Gibson & Nordsieck 2003), resulting in $\Delta K > 0.1$ mag. Considering that this is above the uncertainty of our photometry, red $K-[24]$ color due to obscuration may be misinterpreted as a weak 24 μm excess. Therefore, we corrected the V and K magnitudes for extinction. The extinction values reported in Tables 1 and 2 are either from the Pleiades catalog or have been derived by us for members with known spectral types. We calculated reddening using $V-K$ and $J-K$ intrinsic colors for dwarfs tabulated in Bessell & Brett (1988)

TABLE 2

PLEIADES MEMBERS WITH RELIABLE 24 μm PHOTOMETRY

Name	$(V-K)_0$[a] (mag)	$(K-[24])_0$[a] (mag)	F_{24} (mJy)	σF_{24} (mJy)	Spectral Type	A_V (mag)	$v \sin i$[b] (km s^{-1})	Binary?	2MASS
HII 2168.....	−0.32	0.02	210.15	3.10	B8 III	0.09	215	VB, SB1?	03490974+2403121
HII 0563.....	−0.25	−0.18	98.66	0.91	B6 V	0.07	135	SB1?	03451250+2428021
HII 1823.....	−0.18	−0.16	38.06	0.39	B8 V	0.08	270	...	03482081+2325165
HII 2425*	−0.14*	0.69*	45.60*	0.67*	B9 V*	0.10*	310*	...	03494353+2342427*
HII 1431.....	−0.05	0.01	17.26	0.22	A0 V	0.29	40	SB2	03472945+2417180
HII 0717.....	0.02	−0.15	15.17	0.24	A1 V	0.60	15	VB, SB?	03453777+2420083
HII 2181*	0.04*	2.30*	652.41*	3.00*	B8 V pe*	0.13*	340:*	VB*	03491121+2408120*
HII 1084.....	0.05	−0.06	11.53	0.13	A0 V	1.12	150	SB2?	03463420+2337264
HII 1380*	0.10*	0.17*	14.85*	0.27*	A1 V*	0.00*	235*	...	03472096+2348121*
HII 1432*	0.18*	0.85*	1414.24*	20.84*	B7 IIIe*	0.06*	220*	SB1*	03472908+2406184*
HII 0804.....	0.18	−0.06	8.40	0.14	A2 V	0.38	170	SB1	03455163+2402200
Pels 58*	0.27*	1.07*	19.24*	0.34*	A3*	0.21*	95*	...	03455913+2523549*
HII 1876.....	0.39	−0.00	17.26	0.19	A1 V	0.00	105	PHB, SB?	03483009+2420441
HII 1362.....	0.43	0.02	6.71	0.11	A7	0.21	<12	...	03471935+2408208
HII 2195*	0.49*	0.25*	8.59*	0.09*	A7 V*	0.06*	160*	SB?*	03491219+2353126*
HII 1384.....	0.50	−0.04	11.32	0.17	A4 V	0.18	215	...	03472405+2435184
HII 0531.....	0.58	0.03	6.20	0.12	Am?	0.30	75	...	03450653+2415486
HII 1284*	0.65*	0.30*	8.56*	0.13*	A9 V*	0.09*	100*	SB1?*	03470421+2359426*
HII 1266.....	0.67	−0.05	8.40	0.20	A9 V	0.31	95	VB	03470354+2449117
HII 0344.....	0.68	0.03	7.71	0.16	A8 V	0.02	200	...	03442570+2423408
HII 0697.....	0.74	0.04	6.60	0.09	A9	0.21	75	...	03453445+2427478
HII 1762.....	0.80	−0.05	8.10	0.10	A9 V	0.13	180	SB2	03481354+2419063
HII 0975.....	<0.42:	<−0.05:	3.36	0.08	F	>1.86:	32	PHB	03461799+2329119
HII 0530.....	0.95	0.08	4.95	0.10	F3	0.00	<12	...	03450528+2342097
HII 1122.....	0.97	0.09	4.27	0.09	F4	0.15	29	SB2	03463932+2406116
HII 0605.....	0.99	−0.05	5.20	0.09	F3	0.18	80	SB1	03452085+2455194
HII 2345.....	0.99	−0.07	4.21	0.17	F4	0.08	130	...	03493272+2322494
HII 1309.....	1.06	−0.03	3.49	0.11	F6	0.14	85	...	03471005+2416360
HII 1338.....	1.10	−0.04	7.21	0.10	F3	0.11	10:	SB2	03471656+2407420
HII 1200*	1.11*	0.10*	3.11*	0.05*	F6*	0.29*	14*	...	03465053+2314211*[c,d]
HII 1912.....	1.14	−0.03	5.63	0.12	F4	0.16	75	VB	03483480+2410523
HII 1726.....	1.16	0.04	5.16	0.10	F7	0.17	13	IRB 0.57[e]	03480718+2408315
HII 1613.....	1.25	0.02	2.78	0.08	F8	0.07	20	...	03475252+2356286
HII 0727.....	1.27	0.01	3.61	0.08	F9	0.16	50	...	03454016+2437380
HII 0405.....	1.29	0.00	2.89	0.08	F9	0.03	18	...	03444075+2449067
HII 1856.....	1.31	−0.06	2.39	0.07	F8	0.05	15	...	03482616+2402544
HII 2506.....	1.37	−0.06	2.08	0.05	F8	0.10	14	...	03495648+2313071[c]
AK 1B 146	1.40	−0.07	3.56	0.06	F8	0.02	12/9	SB2	03435067+2516081
HII 3179.....	1.42	−0.05	2.43	0.05	G0	0.00	5	...	03515685+2354070[c]
HII 1797*	1.45*	0.47*	3.61*	0.08*	F9*	0.03*	20*	...	03481691+2338125*
HII 1101*	1.45*	0.42*	3.32*	0.05*	F9.5*	0.05	19*	...	03463878+2457346*[c]
HII 1207.....	1.45	0.01	1.90	0.08	G0:V	0.09	5	...	03465491+2447468
HII 1924.....	1.45	0.06	2.20	0.07	G0	0.01	14	...	03483451+2326053
HII 2786.....	1.45	−0.03	2.02	0.05	...	...	22	...	03504007+2355590[c]
HII 0923.....	1.46	0.08	2.72	0.08	G0	0.05	18	...	03461005+2320240
HII 0489*	1.46*	0.21*	2.55*	0.09*	G0*	0.11*	18*	...	03445639+2425574*
HII 0120.....	1.48	0.01	1.71	0.05	G1	0.26	9	SB1?	03433195+2340266[c]
HII 0152.....	1.48	0.13	1.84	0.05	G1	0.14	11	...	03433772+2332096[c,f]
HII 0250.....	1.48	−0.02	1.73	0.06	G1	0.18	7	SB?	03440424+2459233
HII 0293.....	1.48	−0.01	1.77	0.05	G1	0.28	7	...	03441391+2446457
HII 0314.....	1.48	0.10	2.26	0.09	G1	0.20	38	SB1?	03442008+2447461
HII 0996*	1.48*	0.22*	2.41*	0.07*	G1*	0.02*	12*	...	03462267+2434126*
HII 1015.....	1.48	−0.03	1.79	0.05	G1	0.08	10	...	03462735+2508080[c]
HII 1794.....	1.51	0.03	2.09	0.09	...	...	11	...	03481712+2353253
HII 1182.....	1.53	0.01	1.95	0.05	G5	0.00	16	IRB 1.14[e]	03464706+2254525[c]
HII 0739.....	1.58	0.02	5.00	0.08	G0	0.06	14	PHB	03454211+2454215
HII 1514.....	1.58	0.09	2.07	0.07	G5	0.00	14	...	03474044+2421525
HII 2341.....	1.66	0.07	1.61	0.07	G4	0.06	3	...	03493312+2347435
HII 1117.....	1.67	0.07	3.03	0.09	G6	0.00	6/4	SB2	03463767+2347159
HII 0514*	1.68*	0.12*	1.97*	0.05*	...	...	10*	...	03450400+2515282*[d]
HII 2644.....	1.76	−0.03	1.32	0.05	...	...	4	...	03502089+2428003[c]
HII 3097.....	1.80	0.05	1.66	0.05	...	...	15	SB1	03514044+2458594[c]
HII 0571.....	1.85	0.08	1.64	0.05	G8	0.21	8	SB1	03451534+2517221
HII 2311.....	1.92	−0.08	1.15	0.05	...	...	6	...	03492873+2342440
HII 1095*	2.00*	0.27*	1.29*	0.08*	K0*	0.18*	4*	...	03463777+2444517*

TABLE 2—*Continued*

Name	$(V-K)_0$[a] (mag)	$(K-[24])_0$[a] (mag)	F_{24} (mJy)	σF_{24} (mJy)	Spectral Type	A_V (mag)	$v \sin i$[b] (km s^{-1})	Binary?	2MASS
HII 0173.....	2.04	0.06	2.28	0.05	K0	0.00	8/6	SB2	03434841+2511241
HII 2278.....	2.09	0.03	2.21	0.05	...	...	7	VB 0.37[e]	03492570+2456154[c]
HII 2027.....	2.12	0.01	2.20	0.06	K0	0.00	6	SB2, IRB 0.1[e]	03484894+2416027
HII 0174.....	2.25	0.03	1.34	0.04	...	...	90:	...	03434833+2500157
HII 2147.....	2.23	0.12	2.94	0.07	G9	0.00	7/11	SB2	03490610+2346525
HII 2881.....	2.46	−0.02	1.70	0.05	K2	0.03	10	IRB 0.08[e]	03505432+2350056[c]
HII 1298.....	2.49	0.05	0.89	0.07	...	...	6	IRB 1.18[e]	03470678+2342546
HII 1100.....	2.63	0.12	1.45	0.08	K3	0.25	5	VB 0.78[e]	03463726+2420366
HII 2034.....	2.66	−0.01	0.73	0.06	K2.5	0.00	75	...	03484932+2358383
HII 0885.....	2.72	0.11	1.45	0.05	K3	0.00	6	IRB 0.87[e]	03460776+2452004
HCG 0131.....	2.95	−0.02	0.70	0.05	...	...	...	...	03440282+2539228
HCG 0132.....	2.99	0.11	0.93	0.05	...	...	...	...	03440448+2551226
HII 1653.....	3.34	0.20	0.76	0.07	K6	0.00	21	...	03475973+2443528
HCG 0312.....	3.40	0.42	0.58	0.05	...	...	6.5	...	03481729+2430160
HII 1516.....	3.64	0.33	0.73	0.06	...	...	105	...	03474037+2418071
HCG 0154.....	3.98	0.10	0.79	0.06	...	...	75	IRB 4.61[e,g]	03442729+2450382
HCG 0354.....	4.55	0.60	0.63	0.06	...	...	...	...	03490585+2344232

NOTES.—Objects sorted according to $(V-K)_0$. The 24 μm excess candidates are marked by asterisks.
[a] Dereddened where spectral type available.
[b] The two values are for two components in SB2.
[c] 24 μm data from Stauffer et al. (2005).
[d] Excess object according to Stauffer et al. (2005), but the excess is below our adopted 0.15 mag threshold.
[e] In units of arcseconds.
[f] Big offset between 2MASS and MIPS24 positions, likely contaminated with a background object.
[g] Secondary is a background star.

(after converting them into the 2MASS system following transformations in Carpenter [2001]). The following reddening laws have been used: $A_V = 3.1E(B-V) = 3.1E(b-y)/0.74 = A_J/0.282 = A_K/0.112$ (Cambrésy et al. 2002). Extinction in the 24 μm band has been neglected. Large symbols in Figures 3 and 4 represent dereddened magnitudes; small symbols are observed ones, since no spectral type information is available for these fainter members.

Figure 3 shows a color-magnitude diagram for our and Stauffer's combined sample. The upper envelope traces equal-mass binaries. The debris disk candidates (§ 4) are marked; none of them appear to lie on the binary sequence. Nondetected members within the MIPS field of view are shown as dots. One can see that at the age and distance of the Pleiades we are 100% complete at detecting photospheres earlier than K3 (0.8 $M_\odot$), and in the absence of interstellar dust ("cirrus") could potentially sample photospheres as late as ~M2 (0.4 $M_\odot$).

4. EXCESS OBJECTS

Figure 4 shows the color-color diagram we use to identify members with excesses. Only objects with high-quality 24 μm photometry are plotted. The $V-K$ axis represents photospheric colors. The V and K bands are separated far enough in wavelength space to trace temperature/spectral type and hence luminosity and mass for main-sequence stars. The NIR colors alone, although less affected by reddening, provide a smaller magnitude range and become nonmonotonic at the B–A and K–M transitions. The $K-[24]$ color, on the other hand, only weakly depends on the stellar temperature, since both bands fall on the Rayleigh-Jeans tail for objects as cold as early M dwarfs ($T_{\rm eff} > 3200$ K). In the "Vega system" this color should therefore stay close to zero. Significant positive values indicate the presence of a circumstellar component.

Indeed, as Figure 4 shows, the majority of stars between $V-K = 0.05$ and 3 (spectral types A–K5) cluster around $K-[24] = 0$, getting slightly redder with later spectral type. We regard this region as the locus of pure photospheric colors. It can be fitted as

$$(K-[24])_{\rm phot} = 0.034(\pm 0.010)(V-K)_{\rm phot} - 0.038(\pm 0.016).$$

The standard deviation of residuals for the 57 fitted stars is $\sigma(K-[24]) = 0.051$ mag, which is within the random uncertainty of our photometry.

Eleven stars, however, including HII 1101 from Stauffer et al. (2005), lie significantly redward of the nonexcess locus, indicating $K-[24]$ excess above the 3 σ detection level. HII 1095 is another possible excess member, whose larger uncertainty puts it just below the 3 σ confidence level. Two more, HII 1200 (outside of our field of view) and HII 514, may possess weaker excesses according to the photometry of Stauffer et al. (2005). Despite the difference in the integration times (400 s per source in Stauffer et al. [2005] and 80 s in our survey), both studies observe a similar scatter in the $K-[24]$ color for the solar-type "nonexcess" stars: 0.04–0.05 mag from the average zero value. This makes it difficult to prove excesses in these two stars beyond the 3 σ level; only HII 514 would pass the 0.15 mag threshold adopted in this work. All 14 suspected excess candidates are marked in Figure 4 and highlighted in Table 2; they (as well as HII 152) have been excluded from the above fit to nonexcess members. Excesses are seen around all spectral types down to K0 (and possibly mid-K; see Table 1), with values ranging from 0.1 to 0.5 mag for solar-type stars and 0.15–2.3 mag for early-type stars.

Could excess emission arise from a nearby object confused with a Pleiades member? The average offset between MIPS and 2MASS positions for members from Table 2 is 0.″8. Except for HII 514 and HII 1095, which are the faintest excess candidates, the 24 μm positions fall within a $r = 0.''5$ circle around the 0.″8 systematic offset on the ΔR.A. versus Δdecl. plane, together with

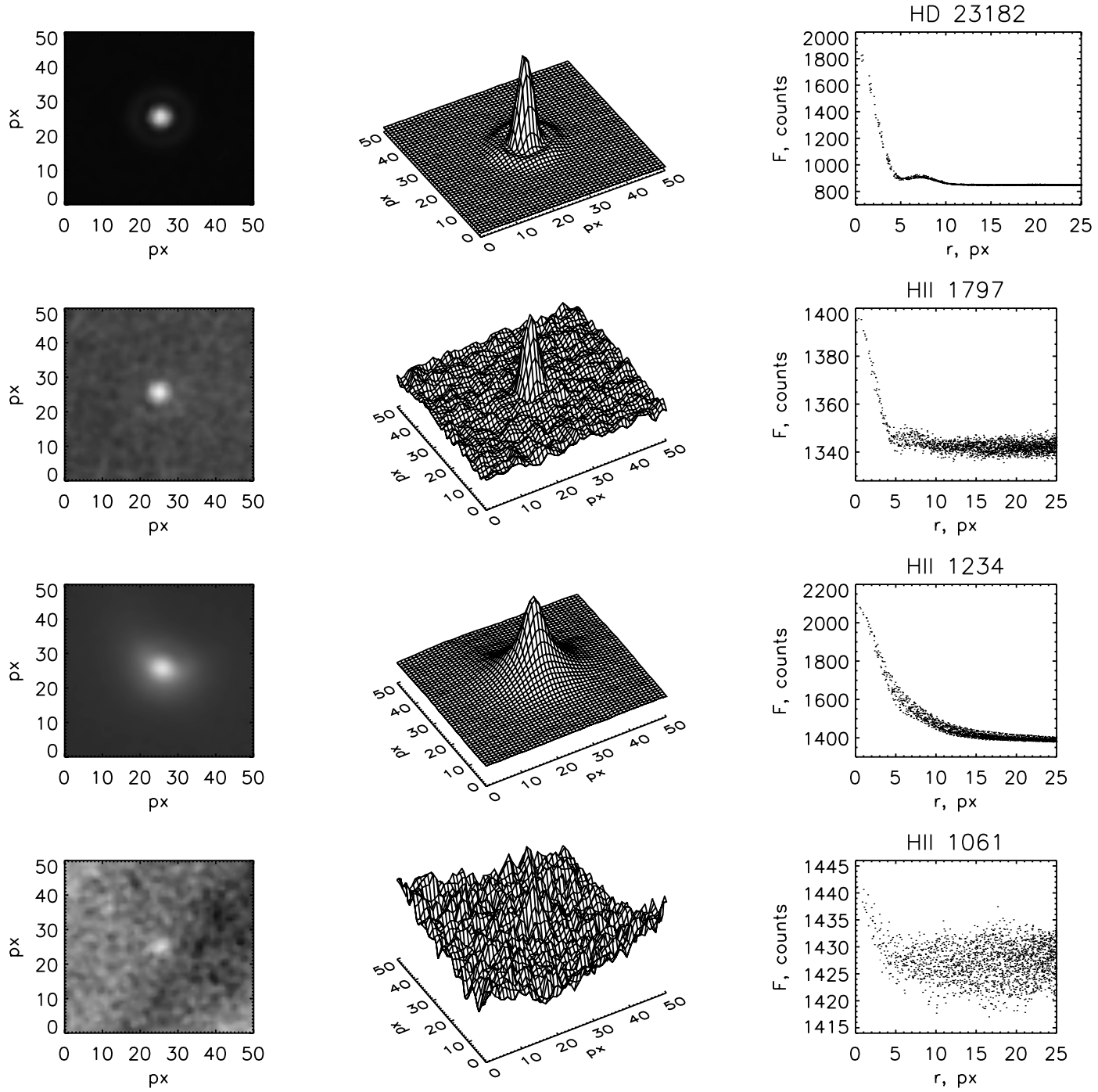

FIG. 2.—Surface and radial plots shown for representative clean and contaminated 24 μm sources. HD 23182, a field star, is one of our PSF templates. HII 1797 is a Pleiades member from Table 2, an example of the sources with well-defined, pointlike profiles. HII 1234 and HII 1061 are from Table 1 and are examples of bright sources with extended smooth halos and of faint sources with nonuniform background, respectively.

the majority of the nonexcess members. Furthermore, they have flux densities above 2 mJy, and the previous studies have shown that the probability of a spurious excess due to chance alignment with a background giant star or galaxy at this flux level is small: $\lesssim$0.1% per source (Gorlova et al. 2004; Stauffer et al. 2005). Due to the proximity of the Pleiades to the ecliptic, however, there is concern about asteroid contamination. We examined images of the detected Pleiades members for the presence of nearby companions without a 2MASS counterpart—signaling a medium-speed asteroid leaving a chain of images as it moves between successive scans. Also, when the object fell in the overlapping region between two fields, we could identify contamination by fast-moving asteroids by comparing two images obtained a few days to a half-year apart. A "close companion" to HII 320 from Table 1 is one such example of likely asteroid contamination, but none are among the 14 excess candidates.

The strongest excess among pointlike sources belongs to HII 2181 (28 Tau, Pleione). The third strongest excess is for HII 1432 (25 Tau, η Tau, Alcyone), the optically brightest member (Fig. 3). Both stars belong to the Be, or "classical," type of emission-line B–A stars. Two other emission stars, HII 468 (17 Tau, Electra) and HII 980 (23 Tau, Merope), may also possess excesses of

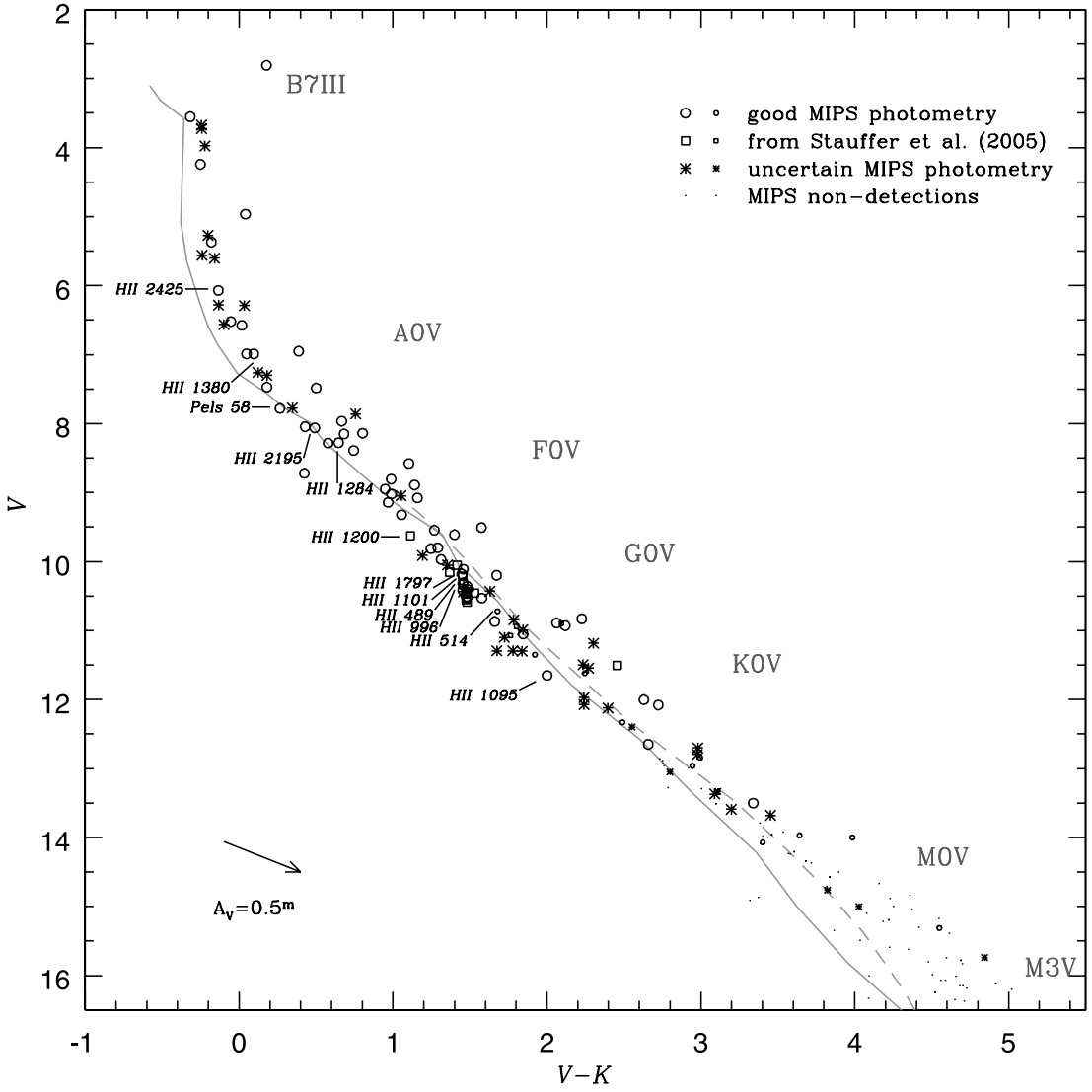

FIG. 3.—Pleiades color-magnitude diagram. *Open symbols*: Clean 24 μm sources from Table 2. *Circles*: This work. *Squares*: Stauffer et al. (2005). *Asterisks*: Contaminated 24 μm sources from Table 1. *Large symbols*: Objects with spectral type, dereddened. *Small symbols*: Objects without spectral type, non-dereddened. *Dots*: 24 μm nondetections. Marked are debris disk candidates according to this work or Stauffer et al. (2005). *Solid line*: 115 Myr isochrone by Siess et al. (2000). *Dashed line*: 125 Myr isochrone by Baraffe et al. (1998). Both isochrones are of solar metallicity and assume a distance of 133.5 pc (Soderblom et al. 2005).

$\sim$0.5 mag, but unfortunately bright nebulosities surrounding these stars make our measurements uncertain (placing them in Table 1). All four are post–main-sequence stars, which is indicated by their giant or subgiant luminosity classes, and fast rotators ($v \sin i > 200$ km s^{-1}). The excess emission is probably free-free emission from gaseous Keplerian disks produced by radiation-driven mass loss and fast rotation (Waters 1986; Porter & Rivinius 2003). The emission stage is episodic—once in about $\sim$10 yr; for reasons still debated, these stars eject a shell that settles into a temporal disk in the equatorial plane. In some cases shell episodes coincide with the periastron passage of a companion (Gies et al. 1990). Mass transfer in a binary system could also account for the spin up of the primary (Harmanec et al. 2002). Pleione is a good example—fastest rotator, with the biggest IR excess and a companion resolved with speckle interferometry (McAlister et al. 1989). On the other hand, any companion to Merope has escaped detection so far (Raboud & Mermilliod 1998); the only indirect evidence for one is the prominent X-ray emission (Daniel et al. 2002).

In the absence of spectroscopic information for the photometrically selected members in clusters other than the Pleiades, debris disk stars can be distinguished from emission-line stars by the absence of excess NIR emission in the former, since even the hottest candidate debris disks have $T < 900$ K (Uzpen et al. 2005). Indeed, none of the rest of the 12 excess members possesses an excess in the 2MASS colors, nor is mentioned as an emission-line star. We therefore regard these stars as debris disk candidates.

The 24 μm images of the nine debris disk candidates discovered in this work are shown in Figure 5; the remaining three are from Stauffer et al. (2005). The central contour is drawn at half the intensity of the brightest pixel on the source, as a measure of the FWHM. As can be seen from these images, the excess emission appears symmetrical and unresolved within the MIPS beam of 6″, meaning that it is confined to $<$800 AU from the parent stars, consistent with the sizes of the nearby debris disks resolved in the mid-IR (Stapelfeldt et al. 2004; Su et al. 2005; Telesco et al. 2005). The remaining contours are drawn at the level of the median sky intensity, representing the quality of the background. In all cases the background is flat or only tilted (HII 489 and HII 1284), but uniform within at least the first Airy ring where we measure the sky level, lending confidence to the reality of the

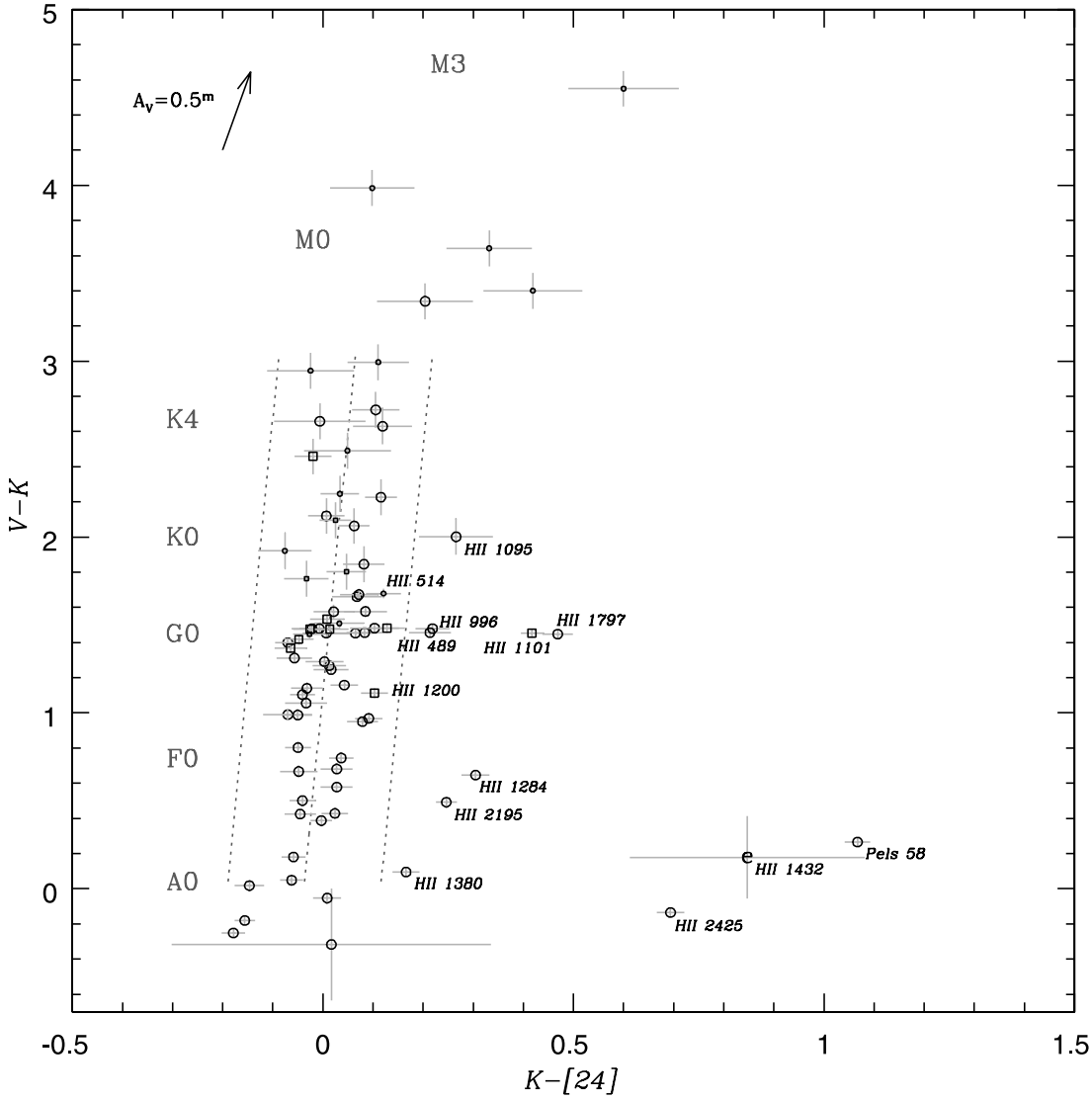

FIG. 4.—Plot of $V-K$ vs. $K-[24]$ diagram identifying excess objects (marked). Only members with good 24 μm photometry (Table 2) are plotted. Symbol coding is the same as in Fig. 3. Symbol "e": Be star HII 1432; another Be star, HII 2181 (Pleione), is off scale at $K-[24] = 2.3$. The V magnitudes are a compilation from Stauffer's catalog; we estimate their errors to be 0.02 mag for B–G stars ($V < 11$ mag) and 0.1 mag for later types; errors in [24] do not include the systematic error of about 5% from uncertainty in aperture correction and in absolute calibration of the 24 μm array. *Dotted lines*: Linear fit to the nonexcess A–K members and ± 3 standard deviations in $K-[24]$ from it.

detected excesses (cf. with the uncertain excess candidates HII 1234 and HII 1061 from Table 1 shown in Fig. 2).

5. PROPERTIES OF THE DEBRIS DISK CANDIDATES

We now discuss individual debris disk candidates in more detail. We arrive at a similar conclusion as Stauffer et al. (2005): except for the 24 μm excess, the host stars for debris disks do not stand out as a group in any other properties. We find, however, that excesses are more frequent among early-type stars and that the solar-type candidates are predominantly single stars.

5.1. *IRAC Excesses*

All disk candidates, except for HII 1095, HII 2425, and Pels 58, have been also imaged with IRAC. None were found to show excess at wavelengths ≤ 8 μm, similar to cirrus-free nonexcess members (Stauffer et al. 2005; J. R. Stauffer et al. 2006, in preparation). This property provides yet another defense against false excesses from heated interstellar material, since in such cases we would expect to detect aromatic emission in the 6–8 μm range.

5.2. *Model Spectral Energy Distributions*

Stauffer et al. (2005) have modeled the spectral energy distribution (SED) from 0.3 to 30 μm in HII 1101. They found that the 24 μm emission arises from an 84 K disk with a central hole 13 AU in radius. Considering that $V-K$, IRAC, and MIPS fluxes of our strongest solar-type disk candidate HII 1797 are very similar to HII 1101, it could be that a similar cold disk is observed in HII 1797 as well, and probably much different from the ones around the F9 dwarf in M47 and M dwarf in NGC 2547 that have much stronger 24 μm excesses (Gorlova et al. 2004; Young et al. 2004). Given the relatively few constraints, a variety of alternative disk models are also likely to be compatible with the SEDs of these stars.

5.3. *Binarity*

One can expect two opposite effects of binarity on debris disks. The circumstellar disks in binaries may be more truncated and the inner part of the circumbinary disk better cleared compared to

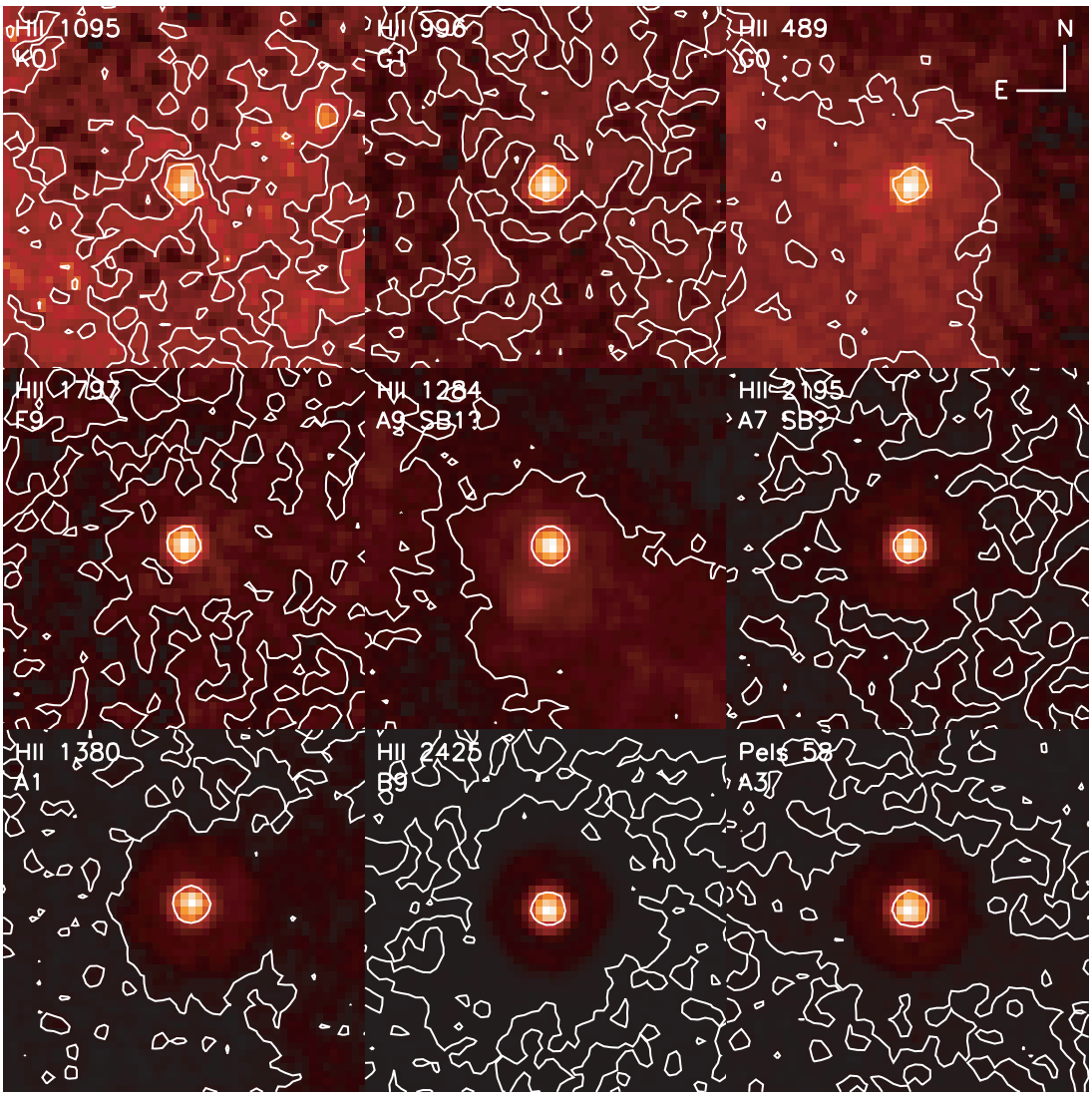

FIG. 5.—Plot of 24 μm images of the debris disk candidates discovered in this work: $64'' \times 64''$ (51 pixels $\times$ 51 pixels), linear flux scale. The central contour is drawn at the half-maximum of the source flux, and the remaining contours are drawn at the median sky level.

the single stars, in which case one expects an anticorrelation between excess and binarity. On the other hand, a companion can stir up the debris disk, prompting more collisions and greater dust production. In the field and for old (>1 Gyr) stars, we find that binary systems may tend toward a higher incidence of 24 μm excess (D. E. Trilling et al. 2006, in preparation). The Pleiades can, in principle, provide a useful comparison at a younger stellar age. We therefore discuss binarity for the Pleiades excess stars.

1. HII 2195 has been suspected to be a spectroscopic binary based on the scatter of the radial velocity measurements (Liu et al. 1991). The number of observations, however, is too small to allow determination of the period. The speckle observations of Mason et al. (1993) did not detect any companion within $0\farcs035$–$1''$ and less than 3 mag fainter than the primary. Raboud & Mermilliod (1998) considered this star to be single. The binarity status therefore remains to be confirmed.

2. As with HII 2195, HII 1284 was identified as a spectroscopic binary without a period in Liu et al. (1991), but no companion was detected in the speckle observations of Mason et al. (1993). Raboud & Mermilliod (1998), however, considered it a single-lined spectroscopic binary and derived a mass for the companion of 0.86 $M_{\odot}$, corresponding to spectral type G–K. Also, the weak X-ray emission detected within $2''$ by *Chandra* is consistent with emission from an "inactive late-type companion" (Daniel et al. 2002). It is interesting that HII 1284 is also a photometrically variable star (V1210 Tau). If indeed it belongs to the γ Dor pulsating type, with $\Delta V = \pm 0.02$ mag and $P = 8$ hr (Martín & Rodríguez 2000), this status could explain some of the radial velocity variations currently assigned to the invisible spectroscopic companion.

3. HII 1101 was suspected to be a photometric and spectroscopic binary in Soderblom et al. (1993), confirmed as a spectroscopic binary in Queloz et al. (1998). It was, however, considered a single star in Raboud & Mermilliod (1998) and most recently in Stauffer et al. (2005). Clearly, the above three stars deserve further spectroscopic monitoring to establish their binarity.

4. HII 1380 was reported as a visual binary in Anderson et al. (1966), but binarity is not mentioned in more recent studies (Liu et al. 1991; Raboud & Mermilliod 1998; Dommanget & Nys 2000; Mason et al. 1993).[3] The position and photometric information in the Washington Double Star Catalog (Mason et al.

[3] Dommanget & Nys (2000) also available via the VizieR Online Data Catalog I/260.

2001) indicate that the companion in question could be HII 1368. The proper motion of the latter, however, as well as its large separation (29″) make it an unlikely cluster member.

5. The rest of the disk candidates—HII 489, 514, 996, 1095, 1200, 1797, and 2425—are apparently single stars, as indicated by radial velocity studies (Liu et al. 1991; Raboud & Mermilliod 1998) and their absence in the *Hipparcos* Visual Double Stars Catalog (Dommanget & Nys 2000). Pels 58 is not mentioned in the above binarity studies, perhaps because it is located 1.°3 away from the core (the northernmost square in Fig. 1). Nevertheless, the consistency of the different radial velocity estimates reported for it in VizieR, and the suggestion of Kharchenko et al. (2004)[4] to consider it a radial velocity standard indicate it to be a single star as well.

We looked at the 2MASS images of the disk candidates for physical companions within 15″ that could have been missed in the optical studies (15″ at the Pleiades distance corresponds to the maximum separation set by the dynamical interactions with other cluster members). In addition, we looked for any other objects within the MIPS beam (6″) whose emission could be confused with the member flux. We found HII 2425 to have companion 11″ northeast, which is visible in the 2MASS *K* band only. HII 1101 has a 2MASS companion 9″ southeast, too faint, however, to identify its nature from the NIR colors. None of the remaining disk candidates have 2MASS counterparts within 15″.

Figure 5 shows that at 24 μm only HII 1284 reveals a companion (11″ to the southeast, at R.A. = $03^{h}47^{m}04^{s}.5$, decl. = $+23^{\circ}59'32''.7$) with $F_{24} = 2.1$ mJy. It is seen at the same location on the east and west subfields obtained a few days apart. The absence of a 2MASS counterpart, meaning $K > 14$ mag, and the small reddening of HII 1284, indicate that, if a Pleiades member, this object would have to be of very low luminosity (M6 or later) with a huge excess. The observed colors are too red for an optically thin debris disk, comparable only to excesses from primordial disks in much younger objects (Lada et al. 2006; Muzerolle et al. 2006). The companion to HII 1284 appears therefore to be an unrelated source.

We conclude that the debris disk candidates in the Pleiades are predominantly single stars. A few cases—HII 1284, HII 2195, and HII 1101—are possible, but unconfirmed, spectroscopic binaries. Thus, our debris disk stars should be directly comparable with the field-star studies of Kim et al. (2005) and Bryden et al. (2006) that apply to predominantly single-star samples.

5.4. *Rotation*

The distribution of Pleiades rotational velocities with temperature/mass is bimodal. The first group includes all spectral types and has the upper envelope of the $v \sin i$ distribution exponentially decaying toward later types, starting from above 300 km s^{-1} in B stars (e.g., Pleione) to 7 km s^{-1} in K, to 3 km s^{-1} in early M stars. The second group consists of late-type ultrafast rotators, with velocities of 25–140 km s^{-1} (Stauffer et al. 1984; Soderblom et al. 1993; Queloz et al. 1998). All excess stars fall into the first rotation group formed by the majority of members. With the limited number statistics per spectral bin, we do not find significant correlation of the strength of the 24 μm excess with rotation. For example, the early members HII 2425 and HII 1380 share similar spectral types and fast rotation, but their excesses are markedly different. Half of the late-type ultrafast rotators fall in the region of heavy cirrus (R.A. $< 03^{h}48^{m}$; see Fig. 1), making reliable measurement of their excesses impossible. The remaining are HII 2034, HII 1516, HCG 154, and possibly HII 174, none of which have an excess.

5.5. *X-Rays*

Recent X-ray studies by *Chandra* (Daniel et al. 2002) and *XMM-Newton* (Briggs & Pye 2003) surveyed areas in the cluster core just eastward of the heavy cirrus. The *XMM-Newton* field is a $30' \times 30'$ area northeast of Alcyone and Maia. Except for the late K dwarfs HII 1110 and HII 1280, within this field we detect at 24 μm all nine B9.5–K members detected also in X-rays, as well as two X-ray nondetections, the early A stars HII 1431 and HII 1028. None of these stars show convincing IR excess. Two of them are possibly contaminated: HII 1234 is embedded in a smooth 0.′5 halo, while HII 1028 is somewhat extended for a point source. The *Chandra* field is an adjacent $16' \times 16'$ area between Alcyone and Merope. There are eight B6–K6 common detections between MIPS and *Chandra*, and two nondetections—the A stars HII 1362 and HII 1375. Because this area is strongly affected by cirrus, only three objects have reliable 24 μm photometry. Two of them, the mid-F spectroscopic binaries HII 1122 and HII 1338, do not have 24 μm excess. The third one, HII 1284, A9, is one of the 12 debris disk candidates. The X-ray emission is presumably coming from the spectroscopic inactive late-type companion (Daniel et al. 2002). Among five objects with questionable photometry, three may have 24 μm excesses: the Be star HII 980, A7 HII 956, and K5 HII 1061, all of which are suspected binaries. *ROSAT* observations are less sensitive but more complete in terms of the covered area. Micela et al. (1999) and Stauffer et al. (2005) provided X-ray fluxes for all the solar-type debris candidates (with upper limits for HII 1095 and HII 1200) and upper limits for B–A candidates (except for Pels 58).

Chen et al. (2005a) noted a possible anticorrelation between X-ray activity and debris disk presence, interpreting it as evidence for dust clearing by stellar wind drag. To test this correlation, we plot X-ray luminosities for the solar-like Pleiades members from Table 2 in Figure 6. The sizes of the circles represent the magnitude of the 24 μm excesses. As one can see, the disk candidates are not distinguishable from the diskless ones in this diagram (in agreement with Stauffer et al. [2005]). Although we do not confirm the Chen et al. (2005a) finding, a larger sample is needed for a better test. In addition, the Pleiades stars are significantly older than the members of the Sco-Cen association studied by Chen et al., and the wind drag must be less effective because the stellar wind is weaker.

6. LIFETIME OF THE 24 μm EXCESS

We now compare the excess rate for the Pleiades stars with results from other studies. Various authors use slightly different criteria to define a significant excess, dictated mainly by the precision of their IR measurements, and split their samples into slightly different spectral type/color bins, which are usually limited by the volume and detection limits of a given survey. Spectral type and binarity information are not available for the majority of cluster stars either. For a preliminary comparison with other studies, we define those Pleiades members to have excesses that deviate by more than 0.15 mag ($\sim 3\ \sigma$) from the $K-[24]$ locus of nonexcess members as derived in § 4. We calculate excess frequencies in the following spectral type groups defined with colors (dereddened where possible): (1) early-type stars: B–A, or $V-K \leq 0.8$; (2) solar-type stars: F–K3, $0.8 < V-K \leq 2.7$. We further compute excess fractions separately for single stars. In all cases only stars from Table 2 are used. For our total sample

[4] Also available via the VizieR Online Data Catalog III/239.

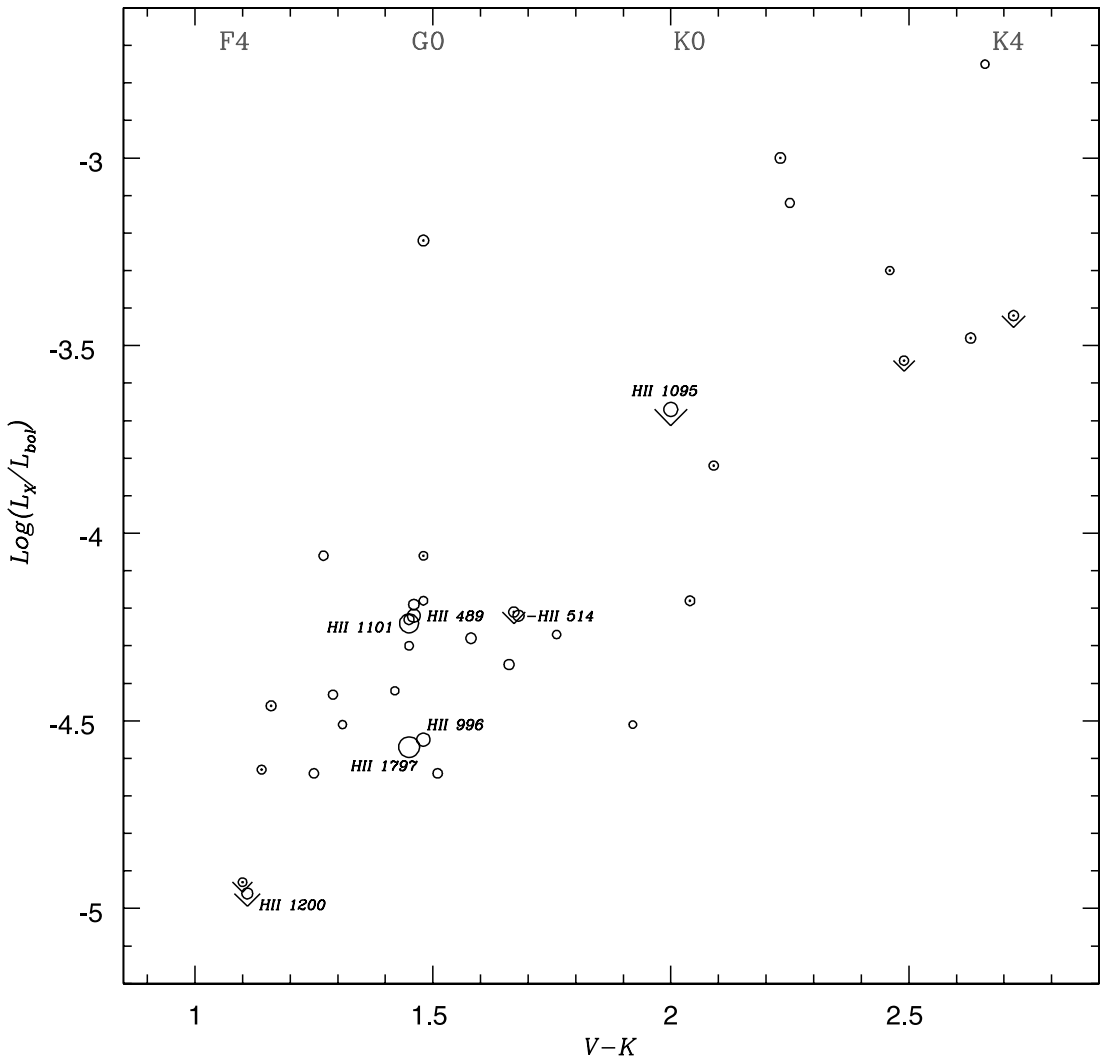

FIG. 6.—Solar-type members from Table 2 with X-ray luminosity fractions from Micela et al. (1999) and Stauffer et al. (2005). *Dotted circles*: Binaries. *Downward-pointing arrows*: Upper limits. Larger circles correspond to bigger $K-[24]$ excess (defined as the deviation from the fit to the nonexcess locus in § 4). Marked are disk candidates. The three strongest single X-ray emitters are the fast rotators HII 727, HII 174, and HII 2034.

of nonemission *early-type* Pleiades stars we obtain an excess fraction of 25% (5 stars out of 20); for a subsample of single stars it is 33% (3/9). For *solar-type* stars we obtain correspondingly: 10% (4/40) based on our measurements only, 9% (5/53) when we include the 13 stars from Stauffer et al. (2005), and for the single stars only in the combined sample: 17% (5/30). Note that a 0.06 mag difference in [24] between us and Stauffer et al. (2005) puts HII 514 just below the boundary between excess and nonexcess objects. Our 0.15 mag excess threshold also eliminates HII 1200 as an excess candidate, so we add only HII 1101 from Stauffer et al. (2005) as having a confirmed excess.

In Table 3 we compile *Spitzer* results on the 24 μm excess fractions in several young clusters and associations and in the field, separately for early-type and solar-type stars. They are binned into several age categories that roughly correspond to the main episodes of dust production in the solar system: clearing of the primordial disk and vigorous collisions between growing planetesimals within the first 10 Myr; rare collisions between terrestrial planet embryos (e.g., the Earth-Moon creation at 30 Myr); possible migration of giant planets that stir smaller bodies and initiate collisional cascades (late heavy bombardment at 700 Myr); and finally a constant process of dust production from colliding asteroids and evaporation of comets.

We derive another limit on debris disk excesses using G giants. G giants are tracers of the post–main-sequence evolution of A stars, unlike cooler K–M giants, which are a mixture of stars with a wide range of masses and at various late evolutionary stages. Jura (1990) searched the *IRAS* Point Source Catalog for 60 μm excess emission in G giants. He found no confident excess among 36 giants. This allows estimation of an upper limit ϵ_{up} on the true excess fraction, using the binomial distribution as appropriate for the small number statistics here. At a confidence level of 0.954 (that corresponds to $\pm 2\ \sigma$ in the Gaussian approximation) ϵ_{up} is calculated from $\int_0^{\epsilon_{up}} 37(1-\epsilon)^{36}\, d\epsilon = 0.954$, resulting in $\epsilon_{up} = 0.08$. Based on a larger sample (that includes fainter stars), Plets et al. (1997) found the 60 μm excess fraction to be 0%–3% for G giants, and even less at 25 μm. Kim et al. (2001) reexamined a dozen *IRAS* excesses around G–K giants with *ISO* and found dust to extend at least a few thousand AU (with $T < 100$ K), which excludes a debris disk interpretation. We therefore adopt 8% as a conservative limit on the 25 μm excess fraction from debris disks around evolved stars of a few solar masses. Data from Table 3 are plotted in Figure 7.

An important new result is the high level of excesses at 24 μm for the roughly solar-mass stars in the Pleiades compared to older field dwarfs. For the field dwarf sample, we have combined the

TABLE 3

24 μm Excess Fraction as a Function of Age

Epoch in the Solar System	Age (Myr)	Cluster	Excess Fraction				Reference
			B–A[a]		F–G–K[a]		
Transition from accretion to debris stage	<10	...	44	4/9	...	...	1
	5–20	Sco-Cen	...	...	34–50[b]	14/41	2
	8–10	TW Hya	...	...	29	2/7	3
Terrestrial planet formation	10–24	...	48	10/21	...	...	1
	25–35	NGC 2547	38	8/21	...	...	1, 4
	25–89	...	47	20/43	...	...	1
Giant planet migration, interaction	90–189	...	26	28/108	...	...	1
	60–100	M47	23	8/35	...	...	5
	100–120	Pleiades	25	5/20	9	5/53	6, 7
Late heavy bombardment, asteroid grinding, destruction of comets	190–800	...	12	10/85	...	...	1
	>1[c]	...	...	...	1.2	2/167	8, 9, 10, 11
Giant stage, evaporating of comets in the Kuiper belt, condensation of stellar wind	>800	...	<8	0/36	...	...	12

[a] Value in left column in units of percent.

[b] The observed level of 34% is due to contamination by interlopers; accounting for them can bring the excess fraction to 50%.

[c] In gigayears.

References.—(1) Rieke et al. 2005; (2) Chen et al. 2005a; (3) Low et al. 2005; (4) Young et al. 2004; (5) Gorlova et al. 2004; (6) this work; (7) Stauffer et al. 2005; (8) Beichman et al. 2005; (9) Kim et al. 2005; (10) Bryden et al. 2006; (11) Beichman et al. 2006; (12) Jura 1990 (G giants).

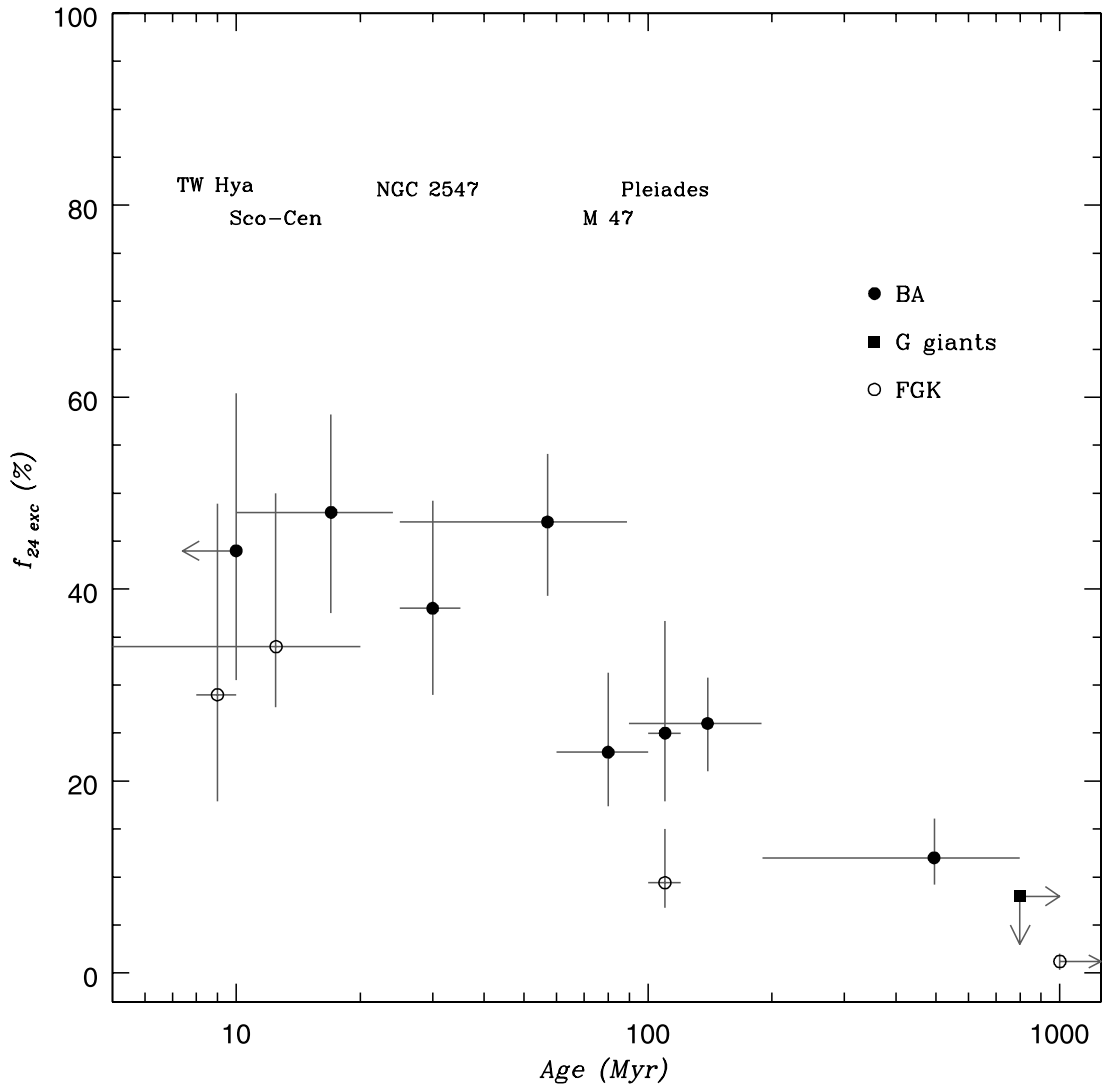

Fig. 7.—Decay of 24 μm excess fraction as a function of age, based on *Spitzer* studies of stars in the young clusters and the field (Table 3). *Filled circles*: Early-type stars. *Open circles*: Solar-type stars. *Filled square*: G giants (descendants of A stars).

work of Kim et al. (2005), Bryden et al. (2006), and Beichman et al. (2006) into a total sample of 167 stars of solar mass and typical age >1 Gyr. Of these stars, two have excesses at 24 μm (HD 69830 and HD 109085), compared with five of 53 solar-mass stars in the Pleiades. We have used the binomial theorem to test the significance of this difference and find a probability of less than 0.3% that the two samples are drawn from the same distribution. That is, 24 μm excesses are more common at 100 Myr than at >1 Gyr at a statistically significant level.

The incidence of Pleiades 24 μm excesses appears to be higher still in stars of $\sim$2.5 $M_{\odot}$ (A stars): 25% versus 9% in solar-mass stars (with a 96% confidence). Does this mean that debris disk masses are systematically greater in high-mass stars? For example, a broad range of masses was found for primordial disks around low-mass stars in Andrews & Williams (2005), which may translate into varying planetesimal masses and give rise to a great variation in debris dust production. However, in the absence of photometry at longer wavelengths, one cannot rule out that the observed difference in excesses is due to the difference in the stellar luminosity or in the SED. More luminous A stars are capable of heating up material to larger distances, resulting in a geometrically larger area that emits at 24 μm. On the other hand, radiation pressure, which is the dominant dust removal mechanism around luminous stars, is also a function of wavelength. Stellar mass and wind are additional factors that enter the expressions for the forces acting on the dust particle (e.g., Chen et al. 2005b). At this time it is not clear which of these effects is the most important cause of the difference. While this observation awaits confirmation from other clusters, the decline in disk fraction with time for both A- and solar-type stars is similar. We thus qualitatively conclude that the disk evolution is similar over the 0.8–2.5 $M_{\odot}$ stellar-mass range and that a significant number of stars within this range are still producing debris at high levels in their planetary zones ($\sim$1–20 AU) at 100 Myr of age.

The apparent difference between field A stars and field solar-type stars arises to first order simply because the A stars are systematically younger. We can therefore use the solar-mass stars as an indication of the evolution of debris disks past the main-sequence lifetime of A stars. Twenty-two of the sample of 167 solar-mass stars discussed above are detected at 70 μm (in general, the observations are deep enough to detect the stellar photospheres, although often at only low signal-to-noise ratio). The rate of detection at this wavelength is 13% $\pm$ 3%, compared with a rate of $\sim$1% at 24 μm. Su et al. (2006) demonstrates, for the field A stars of various ages, and Smith et al. (2006), for nearby B–K young stars, that the 70 μm excess fraction decays slower than the 24 μm one. We conclude that the decline of the 24 μm emission with age corresponds to the decline of the frequency of collisions or disruptive events within the inner parts of the planetary systems, corresponding to the asteroidal zone of the solar system. The outer parts detected at 70 μm, corresponding to the Kuiper Belt zone, evolve more slowly.

Terrestrial planets had formed in the solar system at $\sim$30 Myr (Kleine et al. 2002) and presumably largely cleared material in the inner few AU region that we are probing at 24 μm. However, in different planetary system architectures, Moon-sized bodies within 1 AU may still survive by the Pleiades age of $\sim$115 Myr (Basri et al. 1996). Occasional collisions could give rise to intermittent excesses at 24 μm (Kenyon & Bromley 2005). Another source of warm dust at this age could be occasional disturbances of the asteroid or cometary belts by migrating giant planets. Dynamical simulations show that giant planets can experience strong interactions near the mean motion resonances, resulting in dramatic episodes of scattering and producing a collisional cascade of the smaller bodies, perhaps explaining the Late Heavy Bombardment at 700 Myr in the inner solar system (Gomes et al. 2005; Strom et al. 2005).

Kenyon & Bromley (2005) have quantified this picture in a series of simulations for a solar-type and an A-type star. The predicted evolution of the 24 μm excess can be directly compared to observations from our Figures 4 and 7. After 10 Myr an overall decline in 24 μm excess is predicted, but with levels that are always bigger for the more luminous A stars. Indeed, the *average* excess is observed to decline with age for both early- and late-type stars, and the fraction of detected excesses appears smaller in the solar-type stars compared to the early-type ones (Fig. 7). But how can we explain the observed *range* of excesses between stars of similar age and mass? For solar-type stars, the simulations show it can be explained by collisions within a few AU that produce short-lived excesses in amounts much bigger than the weak preexisting level. For A stars, however, the simulations behave differently: the 24 μm emission comes from distances up to 100 AU, and the excess from a single collision never competes with the excess from the bulk of the disk (cf. Figs. 4 and 8 in Kenyon & Bromley 2005). This result also appears to contradict the observed extent of the Vega system (Su et al. 2005). Therefore, explaining disk behavior as a function of stellar mass is an area requiring further investigation.

7. CONCLUSIONS

We have conducted a photometric survey for warm dusty disks in the Pleiades, the nearest medium-age ($\sim$100 Myr) open cluster. At this age, terrestrial planet formation should be complete, and the inner few AU region is expected to be largely cleared of dust. The dust, however, can be temporarily replenished, either from occasional asteroid collisions or from the outer regions where giant planet migration may still be occurring. Indeed, we find 24 μm excess emission around nine B9–K0 nonemission stars. The fraction of B–A stars with excesses is 25%, comparing well to a similar age cluster M47 (Gorlova et al. 2004).

Because of the proximity of the Pleiades, for the first time we can explore excesses in solar-mass stars down to the photospheric limit. Combined with the Stauffer et al. (2005) sample, we find that the incidence of 24 μm excesses for these stars, at 10%, is significantly higher than that for old field solar-mass stars, 1%. Thus, the clearing of debris in the planetary zone ($\sim$1–20 AU) for these stars takes a similar time as the similar process in A stars, of order 100 Myr. Comparing with the incidence of 70 μm excess in >1 Gyr old solar-mass stars, 13% $\pm$ 3%, it appears that the outer, Kuiper Belt–like zones of planetary debris clear much more slowly that the planetary zones seen at 24 μm.

We would like to thank the referee for comments that helped clarify the paper. This work was supported by JPL/Caltech under contract 1255094.

REFERENCES

Anderson, C. M., Stoeckly, R., & Kraft, R. P. 1966, ApJ, 143, 299
Andrews, S. M., & Williams, J. P. 2005, ApJ, 631, 1134
Arny, T. 1977, ApJ, 217, 83
Backman, D. E., Dasgupta, A., & Stencel, R. E. 1995, ApJ, 450, L35
Backman, D. E., & Paresce, F. 1993, in Protostars and Planets III, ed. E. Levy & J. I. Lunine (Tucson: Univ. Arizona Press), 1253
Baraffe, I., Chabrier, G., Allard, F., & Hauschildt, P. H. 1998, A&A, 337, 403
Basri, G., Marcy, G. W., & Graham, J. R. 1996, ApJ, 458, 600

Beichman, C. A., et al. 2005, ApJ, 622, 1160
———. 2006a, ApJ, 639, 1166
———. 2006b, ApJ, in press
Bessell, M. S., & Brett, J. M. 1988, PASP, 100, 1134
Breger, M. 1986, ApJ, 309, 311
———. 1987, ApJ, 319, 754
Briggs, K. R., & Pye, J. P. 2003, MNRAS, 345, 714
Bryden, G., et al. 2006, ApJ, 636, 1098
Cambrésy, L., Beichman, C. A., Jarrett, T. H., & Cutri, R. M. 2002, AJ, 123, 2559
Carpenter, J. M. 2001, AJ, 121, 2851
Castelaz, M. W., Sellgren, K., & Werner, M. W. 1987, ApJ, 313, 853
Chen, C. H., Jura, M., Gordon, K. D., & Blaylock, M. 2005a, ApJ, 623, 493
Chen, C. H., et al. 2005b, ApJ, 634, 1372
Daniel, K. J., Linsky, J. L., & Gagné, M. 2002, ApJ, 578, 486
Decin, G., Dominik, C., Waters, L. B. F. M., & Waelkens, C. 2003, ApJ, 598, 636
Dermott, S. F., Durda, D. D., Grogan, K., & Kehoe, T. J. J. 2002, in Asteroids III, ed. W. F. Bottke, Jr., A. Cellino, P. Paolicchi, & R. P. Binzel (Tucson: Univ. Arizona Press), 423
Dommanget, J., & Nys, O. 2000, A&A, 363, 991
Gibson, S. J., & Nordsieck, K. H. 2003, ApJ, 589, 362
Gies, D. R., McKibben, W. P., Kelton, P. W., Opal, C. B., & Sawyer, S. 1990, AJ, 100, 1601
Gomes, R., Levison, H. F., Tsiganis, K., & Morbidelli, A. 2005, Nature, 435, 466
Gordon, K. D., et al. 2005, PASP, 117, 503
Gorlova, N., et al. 2004, ApJS, 154, 448
Hahn, J. M., Zook, H. A., Cooper, B., & Sunkara, B. 2002, Icarus, 158, 360
Harmanec, P., Bisikalo, D. V., Boyarchuk, A. A., & Kuznetsov, O. A. 2002, A&A, 396, 937
Herbig, G. H., & Simon, T. 2001, AJ, 121, 3138
Hillenbrand, L. A. 2005, in A Decade of Discovery: Planets Around Other Stars, ed. M. Livio, in press (astro-ph/0511083)
Holland, W. S., et al. 1998, Nature, 392, 788
Jura, M. 1990, ApJ, 365, 317
Kalas, P., Graham, J. R., Beckwith, S. V. W., Jewitt, D. C., & Lloyd, J. P. 2002, ApJ, 567, 999
Kenyon, S. J., & Bromley, B. C. 2005, AJ, 130, 269
Kharchenko, N. V., Piskunov, A. E., & Scholz, R.-D. 2004, Astron. Nachr., 325, 439
Kim, J. S., et al. 2005, ApJ, 632, 659
Kim, S. S., Zuckerman, B., & Silverstone, M. 2001, ApJ, 550, 1000
Kleine, T., Münker, C., Mezger, K., & Palme, H. 2002, Nature, 418, 952
Kraemer, K. E., Shipman, R. F., Price, S. D., Mizuno, D. R., Kuchar, T., & Carey, S. J. 2003, AJ, 126, 1423
Lada, C. J., et al. 2006, ApJ, 131, 1574
Lagrange, A.-M., Backman, D. E., & Artymowicz, P. 2000, in Protostars and Planets IV, ed. V. Mannings, A. P. Boss, & S. S. Russell (Tucson: Univ. Arizona Press), 639
Laureijs, R. J., Jourdain de Muizon, M., Leech, K., Siebenmorgen, R., Dominik, C., Habing, H. J., Trams, N., & Kessler, M. F. 2002, A&A, 387, 285
Liou, J.-C., & Zook, H. A. 1999, AJ, 118, 580
Liu, T., Janes, K. A., & Bania, T. M. 1991, ApJ, 377, 141
Low, F. J., Smith, P. S., Werner, M., Chen, C., Krause, V., Jura, M., & Hines, D. C. 2005, ApJ, 631, 1170
Low, F. J., et al. 1984, ApJ, 278, L19
Martín, S., & Rodríguez, E. 2000, A&A, 358, 287
Mason, B. D., Hartkopf, W. I., McAlister, H. A., & Sowell, J. R. 1993, AJ, 106, 637
Mason, B. D., Wycoff, G. L., Hartkopf, W. I., Douglass, G. G., & Worley, C. E. 2001, AJ, 122, 3466
McAlister, H. A., Hartkopf, W. I., Sowell, J. R., Dombrowski, E. G., & Franz, O. G. 1989, AJ, 97, 510
Meyer, M. R., et al. 2004, ApJS, 154, 422
Micela, G., et al. 1999, A&A, 341, 751
Moraux, E., Bouvier, J., Stauffer, J. R., & Cuillandre, J.-C. 2003, A&A, 400, 891
Morbidelli, A., Brown, M. E., & Levison, H. F. 2003, Earth Moon Planets, 92, 1
Moro-Martín, A., & Malhotra, R. 2002, AJ, 124, 2305
Muzerolle, J., et al. 2006, ApJ, 643, 1003
Pinfield, D. J., Dobbie, P. D., Jameson, R. F., Steele, I. A., Jones, H. R. A., & Katsiyannis, A. C. 2003, MNRAS, 342, 1241
Plets, H., Waelkens, C., Oudmaijer, R. D., & Waters, L. B. F. M. 1997, A&A, 323, 513
Porter, J. M., & Rivinius, T. 2003, PASP, 115, 1153
Queloz, D., Allain, S., Mermilliod, J.-C., Bouvier, J., & Mayor, M. 1998, A&A, 335, 183
Raboud, D., & Mermilliod, J.-C. 1998, A&A, 329, 101
Rieke, G. H., et al. 2004, ApJS, 154, 25
———. 2005, ApJ, 620, 1010
Siess, L., Dufour, E., & Forestini, M. 2000, A&A, 358, 593
Smith, P. S., Hines, D. C., Low, F. J., Gehrz, R. D., Polomski, E. F., & Woodward, C. E. 2006, ApJ, 644, L125
Soderblom, D. R., Nelan, E., Benedict, G. F., McArthur, B., Ramirez, I., Spiesman, W., & Jones, B. F. 2005, AJ, 129, 1616
Soderblom, D. R., Stauffer, J. R., Hudon, J. D., & Jones, B. F. 1993, ApJS, 85, 315
Spangler, C., Sargent, A. I., Silverstone, M. D., Becklin, E. E., & Zuckerman, B. 2001, ApJ, 555, 932
Stapelfeldt, K. R., et al. 2004, ApJS, 154, 458
Stauffer, J. R., & Hartmann, L. W. 1987, ApJ, 318, 337
Stauffer, J. R., Hartmann, L., Soderblom, D. R., & Burnham, N. 1984, ApJ, 280, 202
Stauffer, J. R., et al. 2005, AJ, 130, 1834
Strom, R. G., Malhotra, R., Ito, T., Yoshida, F., & Kring, D. A. 2005, Science, 309, 1847
Su, K. Y. L., et al. 2005, ApJ, 628, 487
———. 2006, ApJ, in press
Telesco, C. M., et al. 2005, Nature, 433, 133
Uzpen, B., et al. 2005, ApJ, 629, 512
Waters, L. B. F. M. 1986, A&A, 162, 121
White, R. E. 2003, ApJS, 148, 487
Young, E. T., et al. 2004, ApJS, 154, 428
Zuckerman, B. 2001, ARA&A, 39, 549
Zuckerman, B., & Becklin, E. E. 1993, ApJ, 414, 793